ExoMol molecular line lists – XLII. Rovibronic molecular line list for the low-lying states of NO

Qianwei Qu [ID], Sergei N. Yurchenko and Jonathan Tennyson [ID]*

Department of Physics and Astronomy, University College London, Gower Street, London WC1E 6BT, UK

ABSTRACT

An accurate line list, called XABC, is computed for nitric oxide which covers its pure rotational, vibrational and rovibronic spectra. A mixture of empirical and theoretical electronic transition dipole moments are used for the final calculation of $^{14}N^{16}O$ rovibronic $A\,^2\Sigma^+ – X\,^2\Pi$, $B\,^2\Pi – X\,^2\Pi$, and $C\,^2\Pi – X\,^2\Pi$ which correspond to the γ, β, and δ band systems, respectively, as well as minor improvements to transitions within the $X\,^2\Pi$ ground state. The work is a major update of the ExoMol NOname line list. It provides a high-accuracy NO ultraviolet line list covering the complicated regions where the $B\,^2\Pi$-$C\,^2\Pi$ states interact. XABC provides comprehensive data for the lowest four doublet states of NO in the region of $\lambda > 160\,nm$ ($\tilde{\nu} < 63\,000\,cm^{-1}$) for the analysis of atmospheric NO on Earth, Venus, or Mars, other astronomical observations and applications. The data are available via www.exomol.com.

Key words: molecular data – opacity – astronomical data bases: miscellaneous – planets and satellites: atmospheres .

1 INTRODUCTION

Nitric oxide (NO) is widely distributed in the Universe. The molecule was observed in the atmosphere of Venus (Gérard et al. 2008) and Mars (Cox et al. 2008), where it is one of the emission sources of the UV nightglow (Bougher et al. 1990; Bertaux et al. 2005). Gerin et al. detected transitions of NO in the dark clouds L134N (Gerin et al. 1992) and TMC1 (Gerin, Viala & Casoli 1993). Halfen, Apponi & Ziurys (2001) reported their analysis of transitions of N_2O to NO in the core region of the Sagittarius B2 and evaluated the N/O chemical network. The first detection of extragalactic NO by Martin et al. (2003) helps us to understand the chemistry of galaxy NGC 253. NO has yet to be detected in the atmosphere of an exoplanet but is thought likely to be important in the atmospheres of rocky exoplanets (Chen et al. 2021). The detection of NO in the astronomical objects relies on knowledge of the corresponding spectral lines of the molecule so accurate NO line list plays significant role in the processes.

There are several available high-resolution line lists of the NO $X\,^2\Pi$ ground state. The HITRAN data base by Gordon et al. (2017) is widely used for investigations of the Earth's atmosphere and other room temperature studies. For higher temperature applications, the NO line list in the HITEMP data base has been recently updated (Hargreaves et al. 2019) based upon use of the ExoMol NOname line list (Wong et al. 2017). The CDMS data base by Endres et al. (2016) contains long-wavelength data including lines with hyperfine-structure; data on two vibrational bands of $^{14}N^{16}O$ are available on the CDMS website. Wong et al. (2017) published the NOname lines list as a part of the ExoMol data base (Tennyson et al. 2020). NOname, available for six isotopologues, contains 21 688 states and 2 409 810 transitions for $^{14}N^{16}O$.

The line lists discussed above provide comprehensive coverage of ground state transitions but do not allow for the transitions involving different electronic states. LIFBASE by Luque & Crosley (1999a) is an exception. It contains line lists for the γ ($A\,^2\Sigma^+– X\,^2\Pi$), β ($B\,^2\Pi– X\,^2\Pi$), δ ($C\,^2\Pi– X\,^2\Pi$), and ε ($D\,^2\Sigma^+– X\,^2\Pi$) NO band systems and provides relative cross-sections via an interactive front-end program. However, there are some issues with the LIFBASE data base, which appears to be no longer maintained, such as some bands of high intensities (e.g. $\beta(12, 0)$ and $\delta(2, 0)$) are missing. Due to the strong interactions and curve crossings between its electronically excited state, it is not easy to model the excited states of NO. Similar interactions were also reported in the works discussing other nitrogen oxide e.g. NO_3 (Stanton 2007). To address this problem, we (Qu et al. 2021) proposed a method based on directly diagonalizing a rovibronic matrix using the variational nuclear motion program DUO (Yurchenko et al. 2016). Our model used a diabatic representation to resolve the energy structures of $B\,^2\Pi–C\,^2\Pi$ coupled states. A MARVEL (measured active rotation vibration energy levels) analysis (Tennyson 2007; Tóbiás et al. 2019) was used to produce a set of empirical energy levels of spectroscopic accuracy. These levels were then used by DUO to produce curves and couplings that give an accurate description of the $A\,^2\Sigma^+$, $B\,^2\Pi$, and $C\,^2\Pi$ states for levels up to 63 000 cm^{-1} above the ground state; the previous NOname line list already provides a good spectroscopic model for the $X\,^2\Pi$ state. This new spectroscopic model provides an excellent starting point for computing a line list for the γ, β, and δ band systems of NO.

This work aims to provide a line list which is both accurate and complete covering the rovibrational transitions within the $X\,^2\Pi$ state and the rovibronic transitions belonging to the other three important band systems, i.e. γ, β, and δ as shown in Fig. 1. Rovibronic energy levels and wavefunctions were taken from our published model (Qu et al. 2021). The TDMC of $A\,^2\Sigma^+– X\,^2\Pi$ was taken from the

* E-mail: j.tennyson@ucl.ac.uk
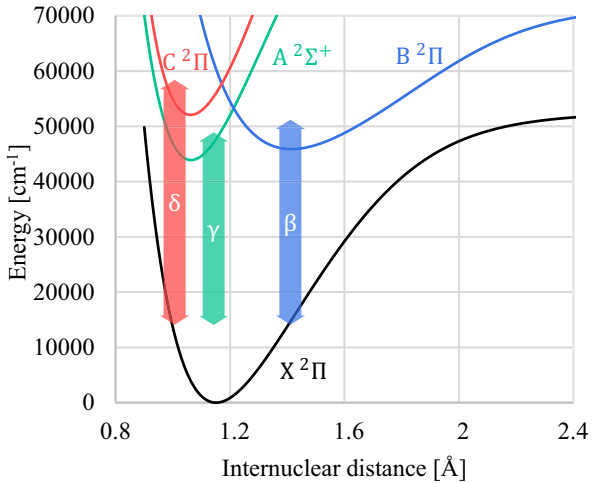
Figure 1. The band systems of NO involved in this work and their names. For a comprehensive diagram, see Cartwright et al. (2000).

literature (Luque & Crosley 1999b), while the $B\,^2\Pi$–$X\,^2\Pi$ and $C\,^2\Pi$–$X\,^2\Pi$ TDMCs, involving two strongly coupled electronic states $B\,^2\Pi$ and $C\,^2\Pi$, are constructed in this work. To make the line list more accurate, some calculated values are replaced with empirical ones and the associated uncertainties were provided. These issues are discussed in turn in the following sections.
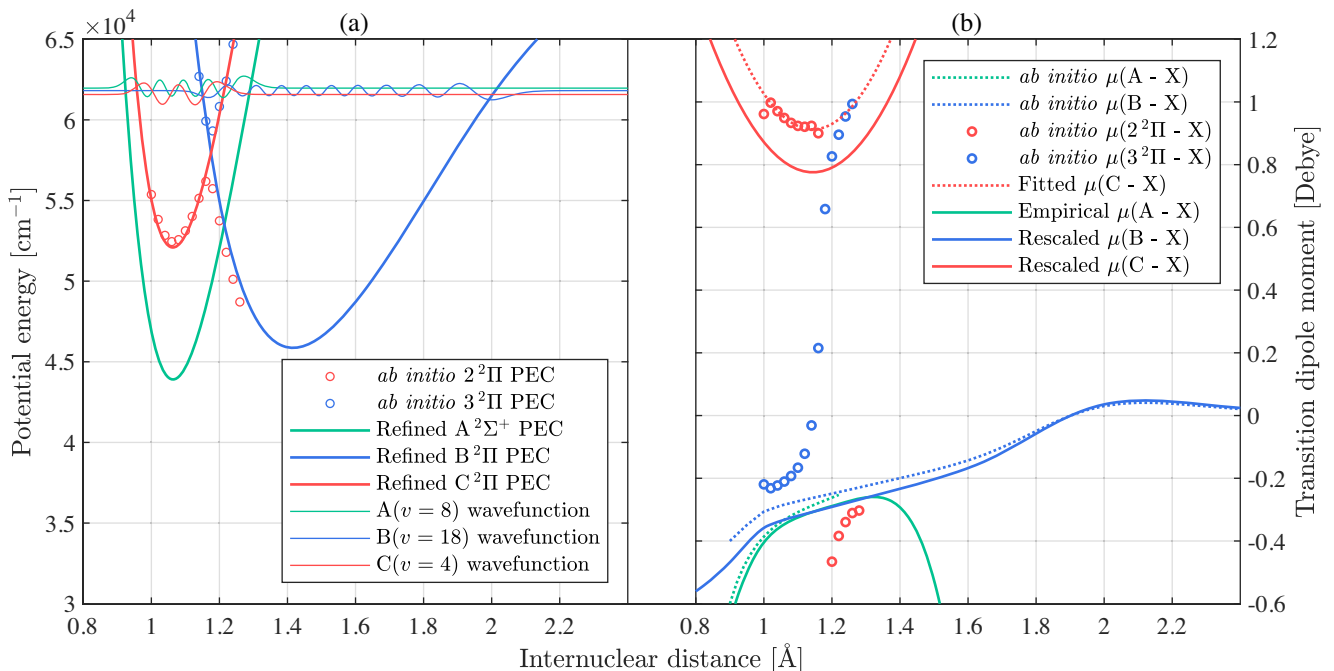
2 TRANSITION DIPOLE MOMENTS

Our previous study (Qu et al. 2021) explored the difficulty of pre-forming ab initio calculations of NO in some detail; fundamentally

the problem arises because the $A\,^2\Sigma^+$ and $C\,^2\Pi$ states are effectively Rydberg-like in character which means their curves follow that of the tightly bound NO^+ ion (Pratt 1998), while the $B\,^2\Pi$ state is a valence state with a much flatter curve which crosses the others, see Fig. 2(a). Discontinuities arise in the potential energy curves (PECs) and other curves due to the state (avoided) crossings and interactions. The quality of transition dipole moment curves (TDMC) is strongly affected by the complicated behaviour of the excited state wavefunctions which were computed at the complete active space self-consistent field (CASSCF) and multireference configuration interaction (MRCI) levels using MOLPRO (Werner et al. 2012). We therefore adopted a pragmatic approach to determining the TDMCs in which the TDMCs were modified through a comparison with experimental data.

2.1 Range of calculation

The calculation setup is consistent with those of Wong et al. (2017) and our previous work (Qu et al. 2021): the internuclear distance, R, varied from 0.6 to 4 Å, which in DUO was discretized by 701 uniformly spaced grid points as part of the sinc DVR (discrete variable representation) basis set. In the final calculations, 60, 15, 30, and 10 contracted vibrational basis functions were retained for the $X\,^2\Pi$, $A\,^2\Sigma^+$, $B\,^2\Pi$, and $C\,^2\Pi$ states, respectively.

As we do not include interactions with higher electronic states (Gallusser & Dressler 1982) in our model, the highest vibrational levels of the $A\,^2\Sigma^+$, $B\,^2\Pi$, and $C\,^2\Pi$ states were limited to 8, 18, and 4, respectively. The vibrational wavefunctions of these levels are shown in Fig. 2(a), where they are vertically shifted to their vibrational energies. The global energy limit was chosen to be $65\,000\,\mathrm{cm}^{-1}$.

Figure 2. (a) Ab initio and refined PECs as well as vibrational wavefunctions and (b) corresponding transition dipole moments, $\mu(\cdot)$. In Panel (a), the wavefucntions are plotted in arbitrary units. $2\,^2\Pi$ is the adiabatic $C\,^2\Pi$ to $B\,^2\Pi$ state and $3\,^2\Pi$ is the adiabatic $B\,^2\Pi$ to $C\,^2\Pi$ state. In Panel (b), 'Fitted $\mu(C-X)$' is a quadratic polynomial which was fitted to the values of red and blue circles it passes through. 'Empirical $\mu(A-X)$' was calculated with the parameters determined by Luque & Crosley (1999b).
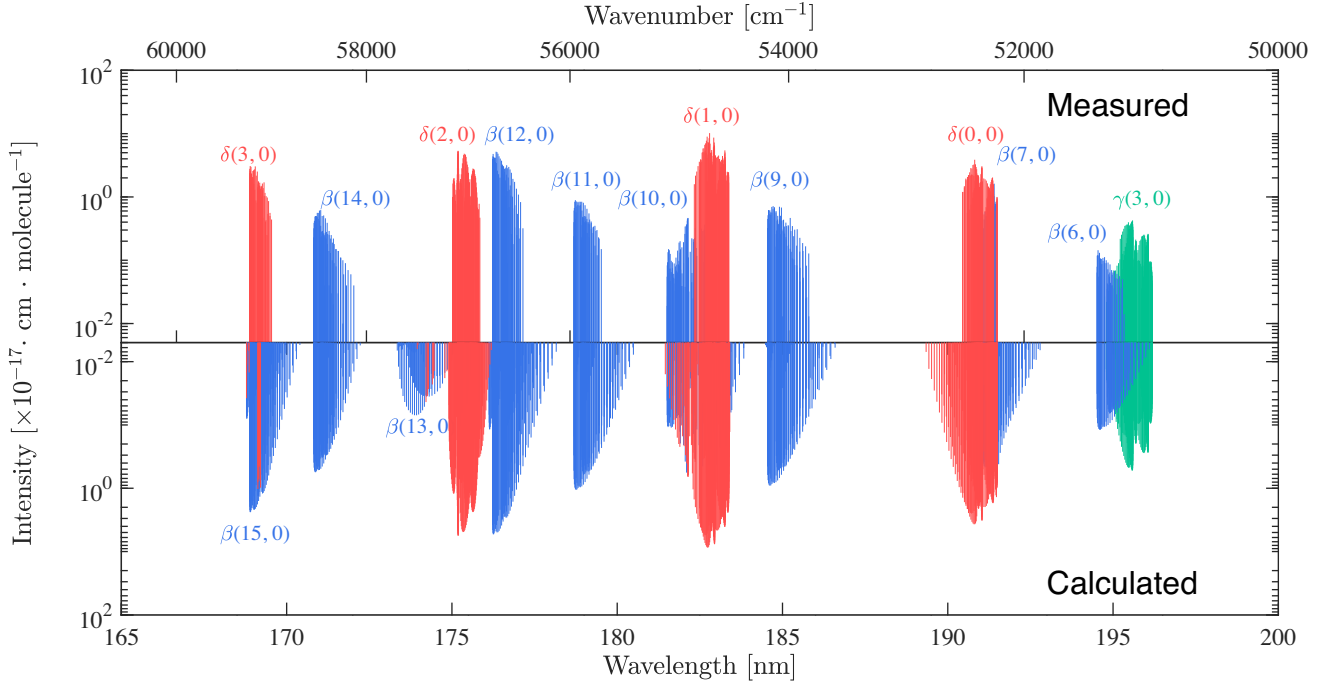
Figure 3. Calculated absorption intensities at 295 K compared with the values given by Yoshino et al. (2006). As the fine-structure doublets for more than half the transitions were not resolved in the experiment, all doublets are removed by averaging the positions of the two lines and adding their intensities, for both measured and calculated transitions.
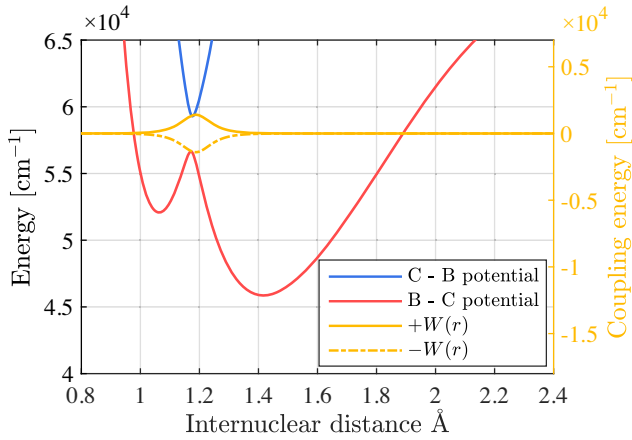
Figure 4. Eigenvalue curves of equation (1).

2.2 A $^2\Sigma^+$ state

For the A $^2\Sigma^+$– X $^2\Pi$ transitions, we used the empirical TDMC constructed by Luque & Crosley (1999b) as a fourth-order polynomial (see the green solid curve shown in Fig. 2(b). We chose not to use an ab initio TDMC of A $^2\Sigma^+$– X $^2\Pi$ although the one depicted by the green dash curve in Fig. 2(b) looks very similar to the empirical one. We found that use of different active spaces in MOLPRO gave TDMCs that were very different in both shape and amplitude; this behaviour is discussed by Sheehy et al. (1994). We thus had to compare these curves with the empirical TDMC and select a similar one; this procedure is neither 'ab initio' nor 'empirical'. The empirical TDMC function of Luque & Crosley (1999b) was based on the lower vibrational levels of the A $^2\Sigma^+$ state. As a result, their polynomial diverges at distances $R > 1.3$ Å. We chose to use this

TDMC unaltered as the vibrational wavefunctions decay rapidly to zero in this region so our line list is insensitive to the behaviour of the TDMC at these values of R.

Settersten, Patterson & Humphries (2009) updated the TDMC polynomial coefficients of Luque & Crosley (1999b) using radiative lifetimes of NO A $^2\Sigma^+$ ($v = 0, 1, 2$) which they measured using time-resolved laser-induced fluorescence. Their transition dipole moment is larger in magnitude than that of Luque and Crosley. We use the TDMC of Luque and Crosley as a balance between measured radiative lifetimes (Luque & Crosley 1999b; Settersten et al. 2009) and the intensities ('integrated cross-section') of the $\gamma(3, 0)$ measured by Yoshino et al. (2006); see Fig. 3.

2.3 B $^2\Pi$-C $^2\Pi$ coupled states

The adiabatic PECs B $^2\Pi$ and C $^2\Pi$ have the same symmetry and therefore form an avoided crossing as shown by our ab initio PECs computed using MOLPRO, see circles in Fig. 2(a). In order to avoid discontinuities in the various curves, including the TDMCs, here we follow our diabatic model (Qu et al. 2021) with the PECs shown in Fig. 2(a). Off-diagonal matrix elements were introduced to represent the electronic state interaction as follows:

$$\begin{pmatrix} V_B(r) & W(r) \\ W(r) & V_C(r) \end{pmatrix}, \tag{1}$$

where $V_B(r)$ and $V_C(r)$ are two diabatic potentials and $W(r)$ is a bell-shaped coupling curve. The effect of this representation is illustrated in Fig. 4, although the above matrix elements are introduced into the rovibronic Hamiltonian matrix rather than directly diagonalizing equation (1) to generate adiabatic potentials shown in this figure.

Due to the (adiabatic) avoided crossing between B $^2\Pi$ and C $^2\Pi$, the adiabatic TDMCs B $^2\Pi$– X $^2\Pi$ and C $^2\Pi$– X $^2\Pi$ exhibit erratic behaviour in the interaction region with their values rising and dropping sharply near 1.18 Å, as shown by the blue and red circles

Table 1. Extract from NO XABC .states file.

i	E	g_i	J	ΔE	τ	g_J	+/−	e/f	state	v	Λ	Σ	Ω	label	E_{DUO}
61	51869.286798	6	0.5	20.000000	4.8551E-02	−0.000767	+	e	X2Pi	49	1	− 0.5	0.5	Sh	51871.759731
62	51970.104351	6	0.5	21.000000	4.3477E-02	−0.000767	+	e	X2Pi	50	1	− 0.5	0.5	Sh	51972.577284
63	52081.384882	6	0.5	22.000000	3.9557E-02	−0.000767	+	e	X2Pi	51	1	− 0.5	0.5	Sh	52083.857815
64	52345.934940	6	0.5	1.050000	5.1915E-07	−0.000767	+	e	B2Pi	7	1	− 0.5	0.5	Ca	52345.934940
65	52372.741033	6	0.5	0.007071	4.4075E-08	−0.000767	+	e	C2Pi	0	1	− 0.5	0.5	Ma	52372.500922
66	53273.412094	6	0.5	0.141421	8.2023E-07	−0.000767	+	e	B2Pi	8	1	− 0.5	0.5	Ma	53273.523369
67	53370.608307	6	0.5	10.050000	1.8421E-07	2.002313	+	e	A2Sigma +	4	0	0.5	0.5	Ca	53370.608307
68	54183.455941	6	0.5	0.020000	5.8924E-07	−0.000767	+	e	B2Pi	9	1	− 0.5	0.5	Ma	54183.325295
69	54690.017247	6	0.5	0.030000	4.0148E-08	−0.000767	+	e	C2Pi	1	1	− 0.5	0.5	Ma	54689.759899
70	55090.440941	6	0.5	0.030000	5.1073E-07	−0.000767	+	e	B2Pi	10	1	− 0.5	0.5	Ma	55090.115548

Notes. i Counting number
E State energy in cm^{-1}
g_i Total state degeneracy
J Total angular momentum
ΔE Energy uncertainty in cm^{-1}
τ Lifetime in s
g_J Lande g-factor
+/−   Total parity
e/f   Rotationless parity
state   Electronic state
v Vibrational quantum number
Λ Projection of electronic angular momentum
Σ Projection of the electronic spin
Ω Projection of the total angular momentum
label Sh for shifted, Ca for calculated, EH for effective Hamiltonian, Ma for MARVEL
E_{DUO} State energy in cm^{-1} calculated with DUO

Table 2. Extract from the NO XABC .trans file.

f	i	A_{fi}	v_{fi}
117	1	3.1174E + 05	44203.001767
129	1	6.4207E + 05	48854.091482
162	1	2.0740E + 05	58538.988402
151	1	1.0243E + 05	53273.417513
156	1	2.5855E + 04	55586.090674
150	1	1.4370E + 06	52372.686268
149	1	2.3080E + 05	52345.937733
134	1	1.4276E + 04	50452.598447
122	1	1.3786E + 02	46503.348087
168	1	5.2902E + 05	61721.081024

Notes. f Counting number of the upper state
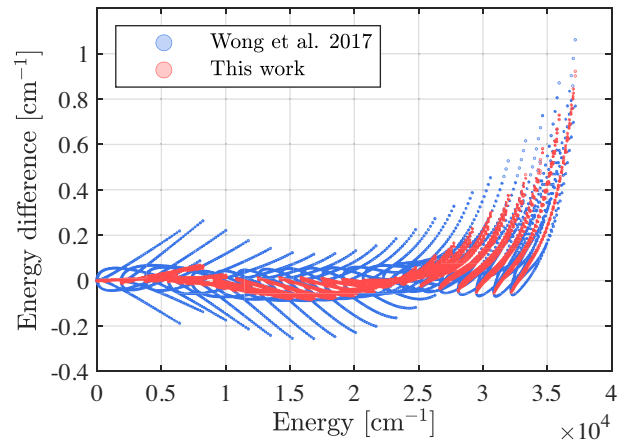i Counting number of the lower state
A_{fi} Einstein-A coefficient in s^{-1}
v Transition wavenumber in cm^{-1}.

Figure 5. Energy differences between the results of DUO and SPFIT/SPCAT for $J \leq 60.5$, $v \leq 20$ states of $X^2\Pi$.

in Fig. 2(b). The interaction centre (about 1.18 Å) is close to the equilibrium bond length (about 1.15 Å) of the $X^2\Pi$ state. Thus, even a slight change in the TDMC in this region along internuclear distance axis can dramatically change the calculated transition intensities.

In the diabatic model, the $B^2\Pi$– $X^2\Pi$ and $C^2\Pi$– $X^2\Pi$ TDMC are smooth curves (see Fig. 2b) which do not show erratic behaviour in the interaction region and therefore are no longer the most sensitive factor in intensity calculations. The coupling between states in this model is controlled by and relies on the quality of the rovibronic $B^2\Pi$ and $C^2\Pi$ wavefunctions, which can be accurately determined by our technique of fitting theoretical curves using experimental energies.

The original ab initio PECs for $X^2\Pi$ and $B^2\Pi$ and the corresponding TDMC of $B^2\Pi$– $X^2\Pi$ were computed using a high level of theory, CASSCF&MRCI + Q/cc-pVQZ with the [(6, 2, 2, 0) − (2, 0, 0, 0)] active space, where $[(n_1, n_2, n_3, n_4) − (n'_1, n'_2, n'_3, n'_4)]$ indicates the occupied and closed orbitals in the irreducible repre-

sentations a_1, b_1, b_2, and a_2 of the C_{2v} point group (shown as red and blue circles in Fig. 2). These adiabatic data were then diabatized to produce curves shown in Fig. 2 as dotted curves. In order to improve the quality of the intensity calculations, the diabtaic TDMCs were then further empirically adjusted as follows. The $B^2\Pi$– $X^2\Pi$ TDMC was scaled using a combination of the measured lifetimes of Luque & Crosley (1995) and integrated cross-sections of Yoshino et al. (2006). The scaling factor of 1.17 was chosen as a balance between these two experiments. The scaled $B^2\Pi$– $X^2\Pi$ TDMC is shown as a blue solid line in Fig. 2. Although the $B^2\Pi$– $X^2\Pi$ TDMC diverges from its original trend for the internuclear distances shorter than 1 Å, this does not affect our calculation as the corresponding $B^2\Pi$ vibrational wavefunctions nearly vanish there.
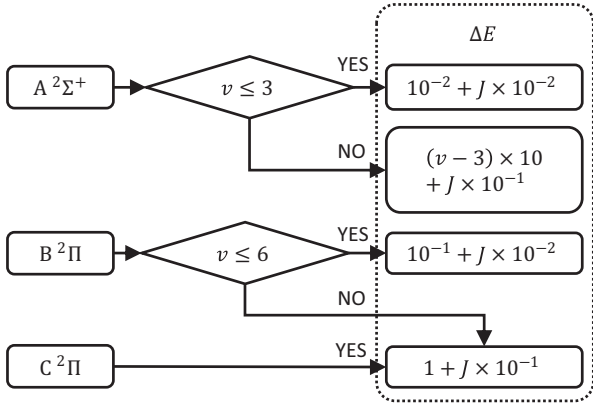
Figure 6. The uncertainties assigned to the calculated energies of A $^2\Sigma^+$, B $^2\Pi$, and C $^2\Pi$ in cm^{-1}.
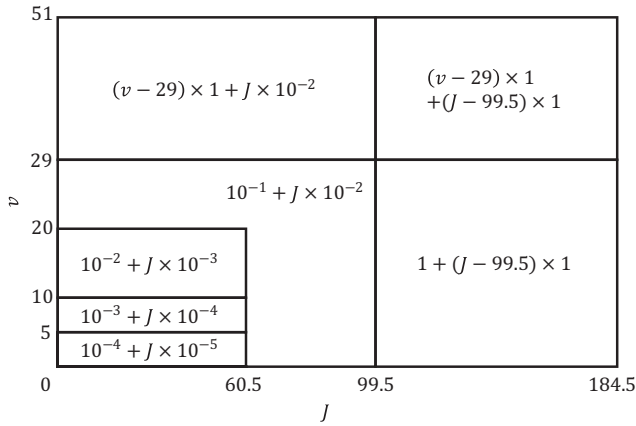
Figure 7. Uncertainties assigned to the energy levels of X $^2\Pi$ state in cm^{-1}. The values are consistent with the recent HITEMP Uncertainty Codes given for NO (Hargreaves et al. 2019).
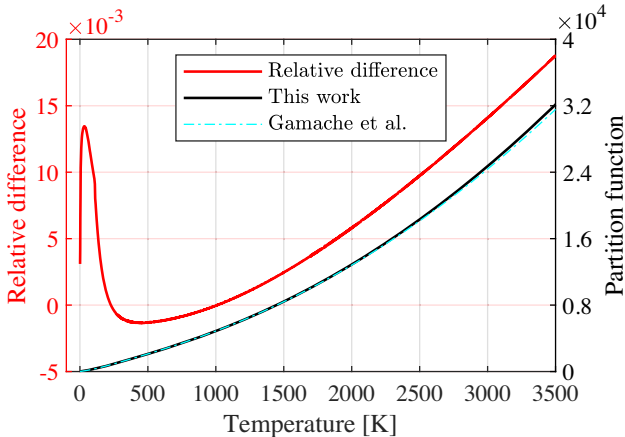
Figure 8. Partition function calculated using the XABC state energies in comparison with the TIPS values of Gamache et al. (2017). The red curve illustrates the relative difference between them.

The TDMC of C $^2\Pi$– X $^2\Pi$ required special care; we first fitted a quadratic polynomial to the adiabatic ab initio values, shown as the red dash curve in Fig. 2, and then scaled it based on the absorption intensities measured by Yoshino et al. (2006). Since the TDMC of C $^2\Pi$– X $^2\Pi$ influences the intensities of higher β bands (i.e. $v_B \geq 7$), it was important to obtain a global agreement for all intensities, including the β system. This is illustrated in Fig. 3, where the calculated spectrum of NO in the region of 200 nm is compared to the experimental intensities by Yoshino et al. (2006).

All curves comprising our spectroscopic mode, including the TDMCs, are provided in the supplementary material to this paper as a DUO input file.
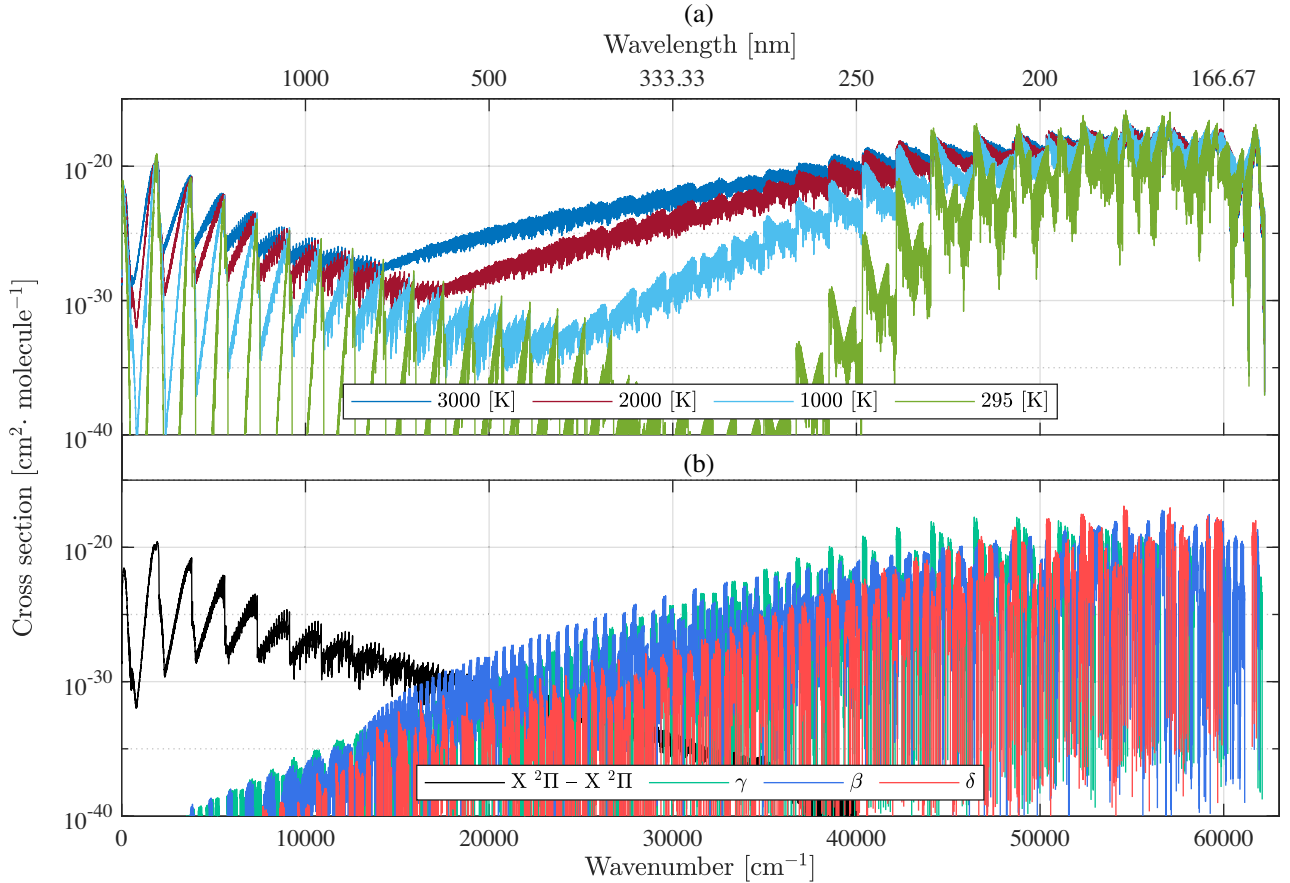
3 LINE LIST CALCULATION

A rovibronic line list XABC for NO was constructed using the DUO program and the spectroscopic model described above. For the detailed description of the DUO calculation see our previous work (Qu et al. 2021).

The XABC line list consists of 4 596 666 transitions between 30 811 states of the four low-lying electronic states X $^2\Pi$, A $^2\Sigma^+$, B $^2\Pi$, and C $^2\Pi$, (21 668, 1209, 6873, and 1041, respectively), covering $J \leq$ 184.5 with rovibronic wavenumber cutoffs of 53 000 cm^{-1} (X $^2\Pi$, same as in Wong et al. 2017) and 63 000 cm^{-1} (all other states). These energy cutoffs are smaller than the basis set limit to avoid any truncation problems near 63 000 cm^{-1}. In line with the ExoMol data structure (Tennyson, Hill & Yurchenko 2013), the line list is represented by two files, a .states (states) file and a .trans (transitions) file. Table 1 gives an extract of the XABC .states file. The .trans (transitions) file contains the Einstein-*A* coefficients calculated with the DUO spectroscopic model of this work and constitutes our new XABC line list. Table 2 gives an extract from the .trans file.

The current spectroscopic model uses improved Λ-doubling parameters for the X $^2\Pi$ state compared to Wong et al. (2017). As a consequence, the new model shows better agreement with the effective Hamiltonian SPFIT/SPCAT energies of NO also presented in Wong et al. (2017), see Fig. 5. Due to the change in the model and consequently the wavefunctions, the Einstein-*A* coefficients between the states of X $^2\Pi$ as well as the corresponding lifetimes have also changed. The energies of the lower rovibronic states ($v \leq 29$ and $J \leq 99.5$) of X $^2\Pi$ were replaced with the NOname ones which were calculated by Wong et al. (2017) using the programs SPFIT and SPCAT (Pickett 1991), based on the work of Müller et al. (2015). These states are labelled with EH to indicate that they were calculated from effective Hamiltonian, which replaces the label e (i.e. empirical) used in NOname for these EH levels. The energies of the other states of X $^2\Pi$ were shifted from the results of DUO, using the same strategy as Wong et al. (2017), to avoid energy jumps above $v = 29$ or $J = 99.5$. These shifted states were labelled with Sh while they were labelled with c (i.e. calculated) in NOname.

We also replaced the DUO energies of the A $^2\Sigma^+$, B $^2\Pi$, and C $^2\Pi$ states with MARVEL energies where available, these states are labelled Ma in the .states file. The jumps between MARVEL and DUO energies in the excited electronic states are negligible. Therefore, we did not shift the other calculated energies of the A $^2\Sigma^+$, B $^2\Pi$, or C $^2\Pi$ states and labelled these states with Ca.

For this line list we also introduced an extra column containing the energy uncertainties (i.e. Column 5, ΔE) for each state. The uncertainties of A $^2\Sigma^+$, B $^2\Pi$, and C $^2\Pi$ were taken from MARVEL analysis where available. Otherwise, they were constructed according

Figure 9. ^{14}N^{16}O cross-sections below 63 000 cm^{-1} calculated using the XABC line list and a Gaussian lineshape function with an HWHM of 1 cm^{-1}: (a) Calculated cross-sections of NO at different temperatures; (b) X$^2\Pi$– X$^2\Pi$, γ, β, and δ cross-sections at 2000 K.

to corresponding vibrational and rotational quantum numbers using the algorithm shown in Fig. 6. The estimation of uncertainties of the X$^2\Pi$ state is a bit more complicated but is based on the same idea, see Fig. 7.

The partition function was computed using the standard summation over energies using levels from our final line list. Fig. 8 compares the Total Internal Partition Sums (TIPS) partition functions, $Q(T)$, of Gamache et al. (2017) and this work. As can be seen from the red curve, i.e. $(Q_{\text{XABC}} - Q_{\text{Gamache}})/Q_{\text{Gamache}}$, the partition function difference is very small because the thermodynamic properties are generally not very sensitive to small variations of higher lying energies as in the X$^2\Pi$ state, while the A$^2\Sigma^+$, B$^2\Pi$, and C$^2\Pi$ energies (not considered in TIPS) are too high to make obvious difference for the temperature below 3500 K considered here.

With the assumption of local thermal equilibrium, we calculated absorption spectra of NO using the new line list XABC. An overview of the XABC absorption spectrum of different temperatures below 63 000 cm^{-1} or longward 1600 Å is shown in Fig. 9.

4 COMPARISONS

Unless otherwise indicated, the following calculations were executed with EXOCROSS (Yurchenko, Al-Refaie & Tennyson 2018), which is a program for generating lifetimes, spectra, partition function etc., from molecular line lists.

4.1 Lifetimes

Lifetimes for individual states of X$^2\Pi$, A$^2\Sigma^+$, B$^2\Pi$, and C$^2\Pi$ are plotted against the energies in Fig. 10. The vibronic lifetimes of A$^2\Sigma^+$ ($v = 0$ to 3) and B$^2\Pi$ ($v = 0$ to 6) are compared with experimental values (where available) in Tables 3 and 4, respectively. The calculated lifetimes of A$^2\Sigma^+$ state agree well with those measured by Luque & Crosley (1999b). As we used their TDMC, the agreement means that DUO gave similar vibrational wavefunctions as the RKR (Rydberg-Klein-Rees) ones they used. Our computed lifetimes for the B$^2\Pi$ state are larger than those of previous works.

The funnel-like shapes of the dependence of lifetimes on the energy shown in Fig. 10(b) are caused by the interactions between the B$^2\Pi$ and C$^2\Pi$ vibronic levels. The lifetimes decrease to much smaller values when rotational quantum numbers are trapped in these funnels. Apart from the electronic state interaction, the observed lifetimes are further shortened by predissociation. The dot-dash lines in Fig. 10 illustrate the first dissociation limit of NO. As the current version of DUO does not allow for predissociation, the calculated lifetimes to the right of the dot-dash lines are expected to be larger than the observed ones. For example, the calculated lifetimes of C$^2\Pi$ are of the order of 10 ns whereas the measured ones can be as short as several nanoseconds (Hart & Bourne 1989).
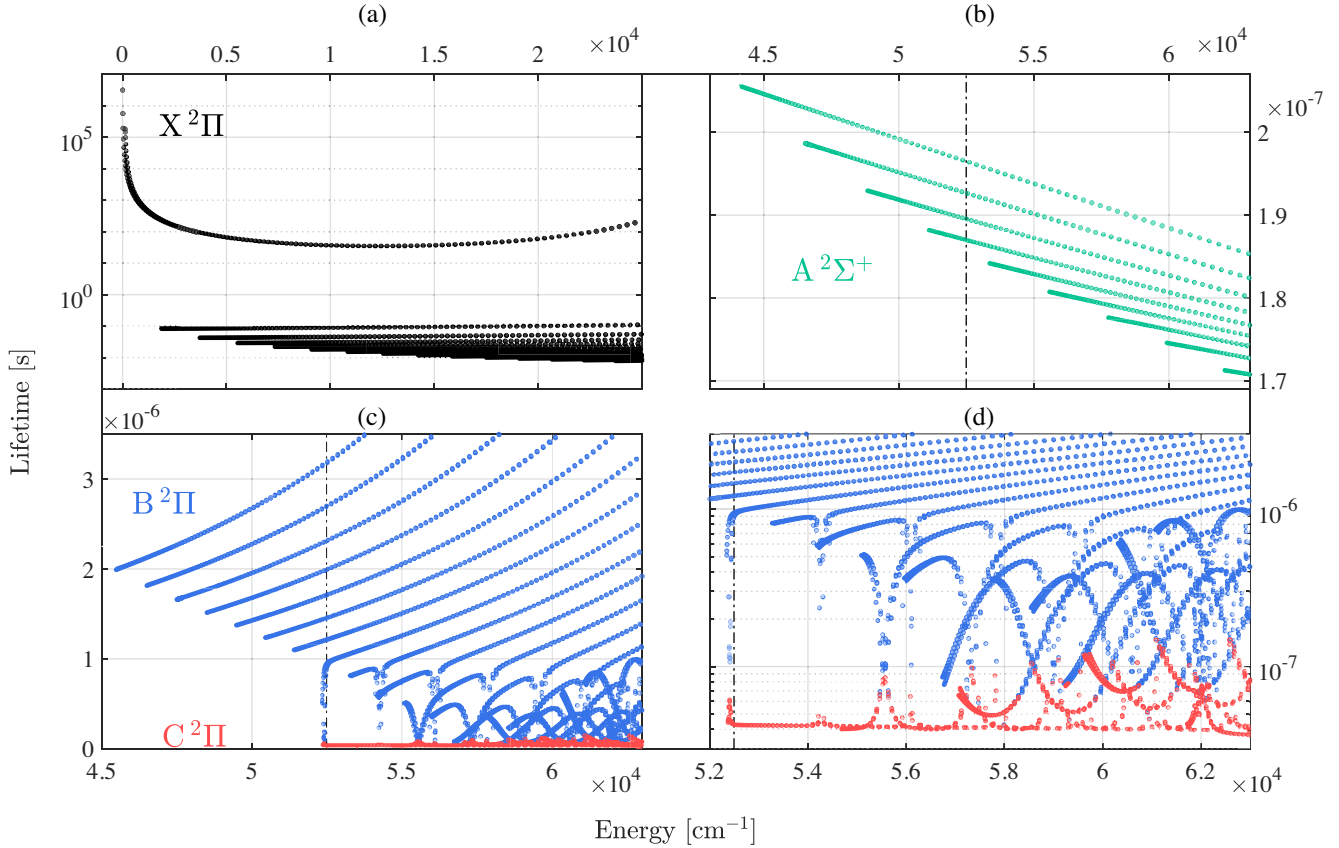
Figure 10. Calculated lifetimes of (a) $X\,^2\Pi$, (b) $A\,^2\Sigma^+$, and (c)&(d) $B\,^2\Pi$–$C\,^2\Pi$ coupled states. The lifetimes of the two lowest states ($X\,^2\Pi$, $v = 0$, $J = 1/2$, $\Omega = 1/2$, e/f) are respectively infinity and 2.3×10^{14} s and are omitted from Panel (a). The vertical dot-dash lines in panels (b), (c), and (d) indicate the first dissociation limit of NO. Panel (d) is a blow up of panel (c).

Table 3. Vibronic radiative lifetimes for the $A\,^2\Sigma^+$ state.

v	Measured (ns)		Calculated (ns)	
	Ref.[a]	Ref.[b]	Ref.[c]	This work
0	205 ± 7	192.6 ± 0.2	206	205.5
1	200 ± 7	186.2 ± 0.4	199	198.6
2	192 ± 7	179.4 ± 0.7	193	192.9
3	184 ± 7	–	188	188.1
4	157 ± 10	–	184	184.1
5	136 ± 10	–	180	180.8

Notes.[a] Luque & Crosley (2000)
[b] Settersten et al. (2009)
[c] Luque & Crosley (1999b)

Table 4. Vibronic radiative lifetimes of $B\,^2\Pi$ state.

v	Measured (μs)	Calculated (μs)	
	Ref.[a]	Ref.[b]	This work
0	2.00	2.00	2.00
1	1.82	1.77	1.84
2	1.52	1.56	1.68
3	1.46	1.39	1.53
4	1.19	1.24	1.38
5	1.07	1.11	1.24
6	0.85	0.99	1.11

Notes.[a] Gadd & Slanger (1990)
[b] Luque & Crosley (1995)

4.2 Absorption spectra

Fig. 11 compares the experimental absorption intensities of $\gamma(3, 0)$ measured by Yoshino et al. (2006) and theoretical intensities calculated with DUO. With the TDMC of Luque & Crosley (1999b), our calculations gives higher intensities than the observed ones for the transitions of $R_{11} + Q_{21}$ and $P_{21} + Q_{11}$ branches. Thus, if we had used the TDMC of Settersten et al. (2009), DUO would further amplify the intensities of all branches, worsening agreement with observation.

The $B\,^2\Pi$–$C\,^2\Pi$ interaction have small effect on the intensities of lower seven $\beta(v', 0)$ bands. Fig. 12 compares the experimental intensities of $\beta(6, 0)$ measured by Yoshino et al. (2006) and theoretical intensities calculated with DUO.

The relative cross-section values calculated by LIFBASE (Luque & Crosley 1999a) are compared with DUO values in Fig. 13. The values of LIFBASE are scaled according to the peak of $\beta(6, 0)$ band.

The $\delta(1, 0)$ band is the strongest one at 295 K in the $B\,^2\Pi$–$C\,^2\Pi$ interaction region and the intensities of the transitions in this band are plotted in Fig. 14. The figure demonstrates the overall agreement between experimental and theoretical values but also exposes defects in our model showing the interaction model for $B\,^2\Pi$ – $C\,^2\Pi$ is not perfect.

Note that, the spectra in Figs 11, 12, and 14 were calculated using the pure DUO energies before they have been replaced by MARVEL
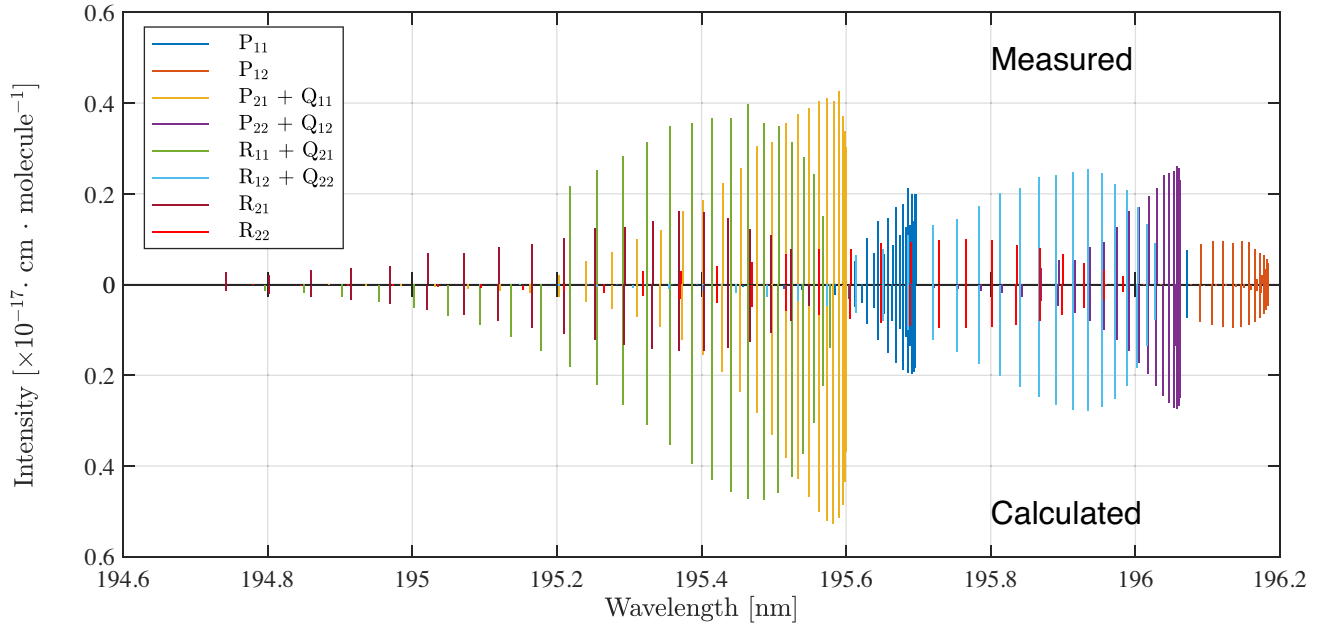
Figure 11. Calculated absorption intensities of the NO $\gamma(3, 0)$ band at 295 K compared with the those published in the work of Yoshino et al. (2006). As no spin-rotational fine structure was observed in the experiment, the wavelengths of the calculated doublets are averaged and their intensities summed, to also give blended lines.
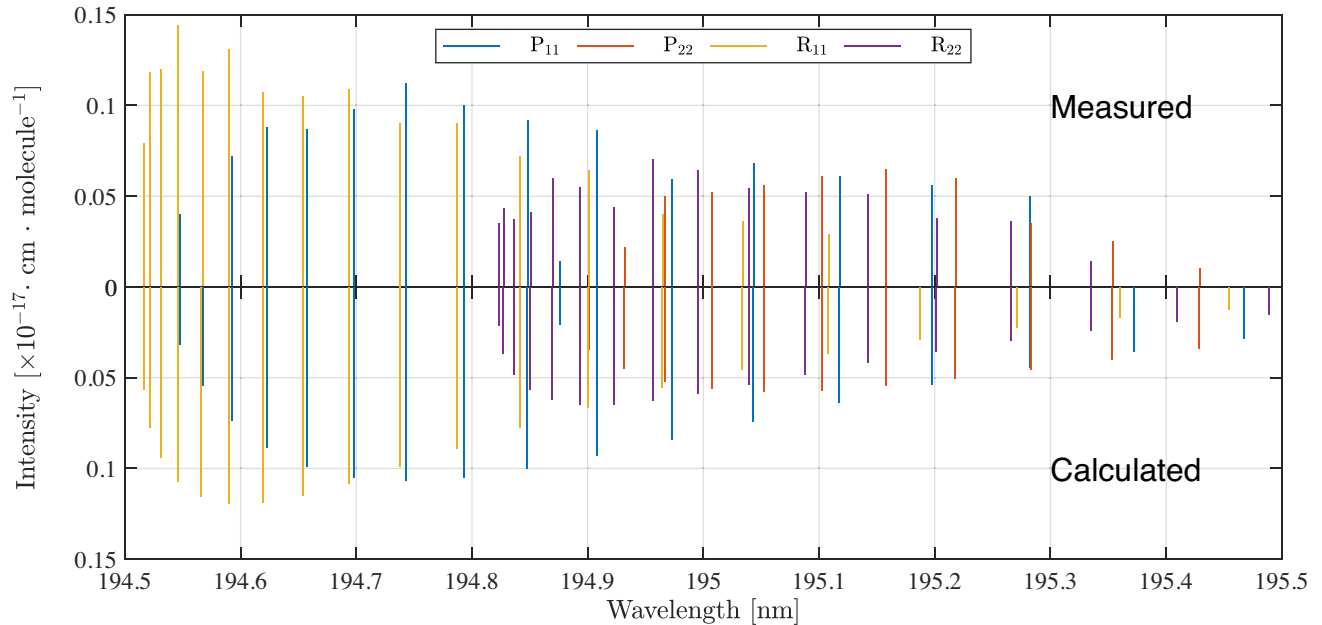
Figure 12. Calculated absorption intensities for the $\beta(6, 0)$ band at 295 K in comparison with the values given by Yoshino et al. (2006). The line intensities of this band are weak and the experiment only resolved the Λ-doublets of high J lines in P_{11} and R_{11} branches. To achieve higher signal-noise ratio, we averaged the wavelengths of the e and f doublets and added up their intensities to create blended transitions for all branches.

or EH values. However the difference between the experimental and calculated lines is indistinguishable at this scale.

5 CONCLUSIONS

Here we present a new line list for $^{14}N^{16}O$ called XABC which covers transitions between the ground electronic state $X\,^2\Pi$ and

the four lowest lying states, $X\,^2\Pi$, $A\,^2\Sigma^+$, $B\,^2\Pi$, and $C\,^2\Pi$. The line list combines effective Hamiltonian (SPFIT), MARVEL, and calculated (DUO) energies, providing high-accuracy line positions. Combined with our $A\,^2\Sigma^+$– $X\,^2\Pi$, $B\,^2\Pi$– $X\,^2\Pi$, and $C\,^2\Pi$– $X\,^2\Pi$ transition dipole moments, the diabatic model predicts the transition intensities which agree well with the measured values. The line list is part of ExoMol project (Tennyson & Yurchenko 2012) and
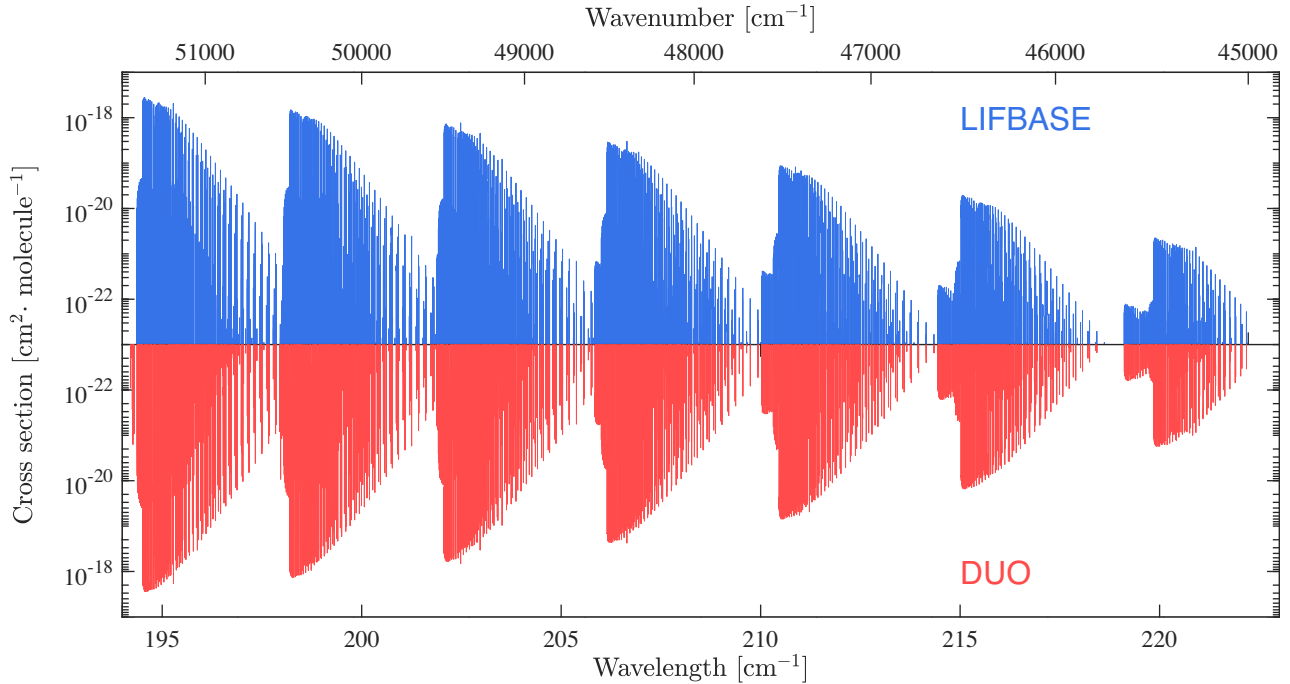
Figure 13. Calculated cross-section of the NO $\beta(v', 0)$ ($v' = 6$ to 0 from left to right) bands of at 295 K in comparison with the data from LIFBASE. The spectrum was computed assuming a Gaussian profile with a half-width-at-half-maximum (HWHM) of 0.2 cm. The relative spectrum simulated by LIFBASE is normalized to the peak of $\beta(6, 0)$ band.
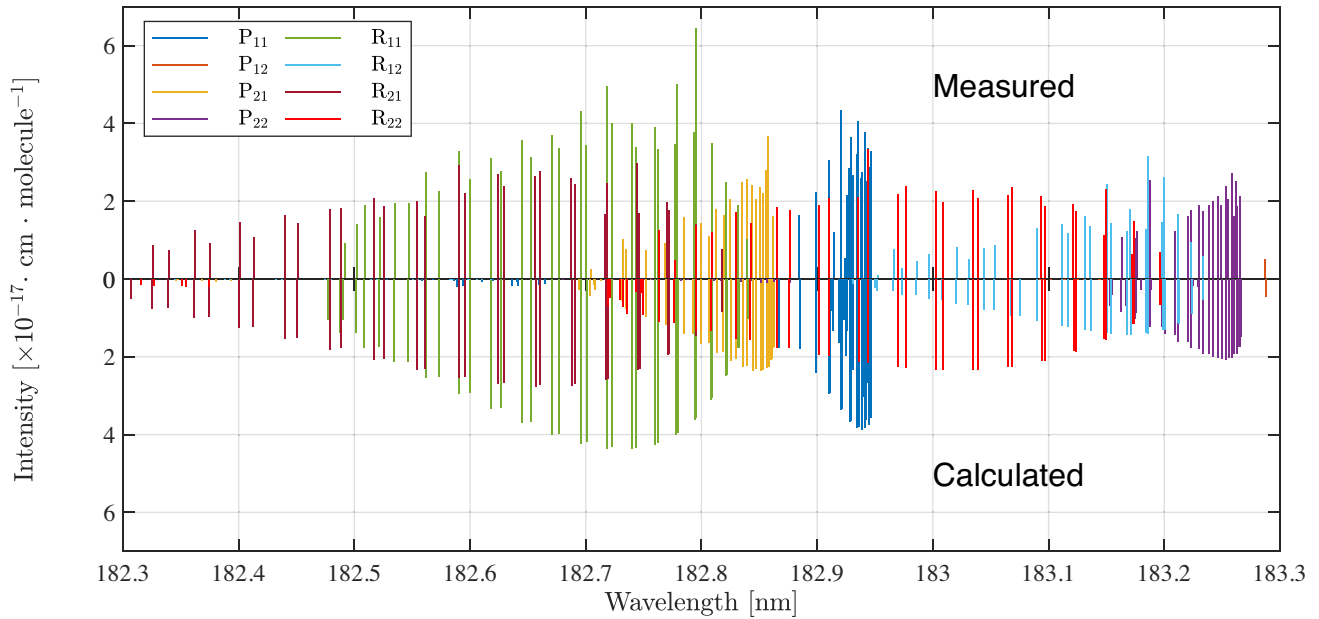
Figure 14. Calculated absorption intensities of the $\delta(1, 0)$ band at 295 K in comparison with the intensities published by Yoshino et al. (2006). This is a strong band and most of the Λ-doublets were resolved in the experiment. To allow comparisons of the fine-structure, we evenly divided the measured intensities of any blended lines to created effective *e*/*f* transitions.

available from www.exomol.com and CDS data base (cdsarc.u-stras bg.fr).

DATA AVAILABILITY

The DUO model file and calculated partition function file are attached as a supplementary materials. The XABC states and transition files of $^{14}N^{16}O$ can be downloaded from www.exomol.com and cdsarc.u-strasbg.fr. The open access programs EXOCROSS and DUO are available from github.com/exomol.

REFERENCES

Bertaux J.-L. et al., 2005, Science, 307, 566
Bougher S. W., Gérard J. C., Stewart A. I. F., Fesen C. G., 1990, J. Geophys. Res.: Space, 95, 6271
Cartwright D. C., Brunger M. J., Campbell L., Mojarrabi B., Teubner P. J. O., 2000, J. Geophys. Res., 105, 20857
Chen H., Zhan Z., Youngblood A., Wolf E. T., Feinstein A. D., Horton D. E., 2021, Nat. Astron., 5, 298
Cox C., Saglam A., Gerard J.-C., Bertaux J.-L., Gonzalez-Galindo F., Leblanc F., Reberac A., 2008, J. Geophys. Res.: Planets, 113, E08012
Endres C. P., Schlemmer S., Schilke P., Stutzki J., Müller H. S. P., 2016, J. Mol. Spectrosc., 327, 95
Gadd G. E., Slanger T. G., 1990, J. Chem. Phys., 92, 2194
Gallusser R., Dressler K., 1982, J. Chem. Phys., 76, 4311
Gamache R. R. et al., 2017, J. Quant. Spectrosc. Radiat. Transf., 203, 70
Gérard J.-C., Cox C., Saglam A., Bertaux J.-L., Villard E., Nehmé C., 2008, J. Geophys. Res., 113, E00B03
Gerin M., Viala Y., Pauzat F., Ellinger Y., 1992, A&A, 266, 463
Gerin M., Viala Y., Casoli F., 1993, A&A, 268, 212
Gordon I. E. et al., 2017, J. Quant. Spectrosc. Radiat. Transf., 203, 3
Halfen D. T., Apponi A. J., Ziurys L. M., 2001, AJ., 561, 244
Hargreaves R. J. et al., 2019, J. Quant. Spectrosc. Radiat. Transf., 232, 35
Hart D., Bourne O., 1989, Chem. Phys., 133, 103
Luque J., Crosley D. R., 1995, J. Quant. Spectrosc. Radiat. Transf., 53, 189
Luque J., Crosley D. R., 1999a, LIFBASE: Database and spectral simulation program, SRI International Report No. MP 99-009. Headquarters 333 Ravenswood Ave Menlo Park, CA 94025 USA
Luque J., Crosley D. R., 1999b, J. Chem. Phys., 111, 7405
Luque J., Crosley D. R., 2000, J. Chem. Phys., 112, 9411
Martin S., Mauersberger R., Martin-Pintado J., Garcia-Burillo S., Henkel C., 2003, A&A, 411, L465
Müller H. S. P., Kobayashi K., Takahashi K., Tomaru K., Matsushima F., 2015, J. Mol. Spectrosc., 310, 92
Pickett H. M., 1991, J. Mol. Spectrosc., 148, 371

Pratt S. T., 1998, J. Chem. Phys., 108, 7131
Qu Q., Cooper B., Yurchenko S. N., Tennyson J., 2021, J. Chem. Phys., 154, 074112
Settersten T. B., Patterson B. D., Humphries W. H., 2009, J. Chem. Phys., 131, 11
Stanton J. F., 2007, J. Chem. Phys., 126, 134309
Sheehy J. A., Bauschlicher C. W., Langhoff S. R., Partridge H., 1994, Chem. Phys. Lett., 225, 221
Tennyson J., 2007, in Lemaire J. L., Combes F., eds, Molecules in Space and Laboratory. Observatoire de Paris, p. 357
Tennyson J., Yurchenko S. N., 2012, MNRAS, 425, 21
Tennyson J., Hill C., Yurchenko S. N., 2013, in Gillaspy J. D., Weise W. L., Podpaly Y. A., eds, 6th International Conference on Atomic and Molecular Data and Their Applications ICAMDATA-2012. AIP, New York, p. 186
Tennyson J. et al., 2020, J. Quant. Spectrosc. Radiat. Transf., 255, 107228
Tóbiás R., Furtenbacher T., Tennyson J., Császár A. G., 2019, Phys. Chem. Chem. Phys., 21, 3473
Werner H.-J., Knowles P. J., Knizia G., Manby F. R., Schütz M., 2012, WIREs Comput. Mol. Sci., 2, 242
Wong A., Yurchenko S. N., Bernath P., Mueller H. S. P., McConkey S., Tennyson J., 2017, MNRAS, 470, 882
Yoshino K., Thorne A. P., Murray J. E., Cheung A. S.-C., Wong A. L., Imajo T., 2006, J. Chem. Phys., 124, 054323
Yurchenko S. N., Lodi L., Tennyson J., Stolyarov A. V., 2016, Comput. Phys. Commun., 202, 262
Yurchenko S. N., Al-Refaie A. F., Tennyson J., 2018, A&A, 614, A131

SUPPORTING INFORMATION

Supplementary data are available at *MNRAS* online.

14N16O_XABC.model.txt
14N16O_XABC.pf.txt

Please note: Oxford University Press is not responsible for the content or functionality of any supporting materials supplied by the authors. Any queries (other than missing material) should be directed to the corresponding author for the article.

This paper has been typeset from a TEX/LATEX file prepared by the author.